



**First-principles study of semicore electron excitation in the electronic energy loss of ZnO for protons**Xu-Dong Zhao,<sup>1</sup> Fei Mao <sup>1,\*</sup> Shi-Ming Li,<sup>1</sup> Bing-Sheng Li,<sup>2</sup> Hong Mao,<sup>3</sup> Feng Wang <sup>4</sup> and Feng-Shou Zhang<sup>5</sup><sup>1</sup>*School of Nuclear Science and Technology, University of South China, Hengyang 421001, China*<sup>2</sup>*State Key Laboratory for Environment-Friendly Energy Materials, Southwest University of Science and Technology, Mianyang, Sichuan 621010, China*<sup>3</sup>*College of Mechanical Engineering, Hunan Institute of Science and Technology, Yueyang, Hunan 414006, China*<sup>4</sup>*School of Physics, Beijing Institute of Technology, Beijing 100081, China*<sup>5</sup>*College of Nuclear Science and Technology, Beijing Normal University, Beijing 100875, China*

(Received 3 June 2021; accepted 17 August 2021; published 1 September 2021)

The electronic stopping power of zinc oxide for protons is presented over a wide range of velocities by using real-time time-dependent density functional theory. We calculated the electronic stopping power of energetic protons for both channeling and off-channeling trajectories, and revealed the microcosmic mechanism of semicore 3*d*-electron excitation in ZnO. In the low-energy regime, the stopping power obtained from channeling geometry is in a quantitative agreement with the measured data, which reproduced not only the experimental threshold velocity of the stopping power, but also the deviation from velocity-proportional electronic stopping power which is considered to be caused by excitation of the tightly bound 3*d* electrons. In the high-energy regime, we examined the impact parameter dependence of semicore 3*d*-electron excitation of ZnO, and showed that the stopping power obtained from off-channeling geometry greatly improves the simulation results in comparison with the channeling results. We also demonstrated that the electronic energy loss of protons is not only related to the number of electrons excited, but also associated with the energy distribution of excited electrons and holes after collisions.

DOI: [10.1103/PhysRevA.104.032801](https://doi.org/10.1103/PhysRevA.104.032801)**I. INTRODUCTION**

The underlying physics for energetic charged particles depositing energy as they are traversing materials has been an important issue [1–4] which is the fundamental basis for understanding ion-solid interactions, and further the energy loss of energetic ions in solids is of great importance in many applications ranging from material science [5] and space electronics [6] to radiotherapy [7,8]. Generally, the stopping power  $S$  defined as the energy loss per unit path length of charged ions is employed to quantify the ability of materials stopping incoming projectiles. The stopping power is conventionally divided into the electronic stopping power  $S_e$ , which transfers the projectile's kinetic energy to the electronic subsystem of target by inelastic collisions with host electrons, and the nuclear stopping power  $S_n$ , transferring the projectile's kinetic energy to the target nuclei by elastic collisions.

A lot of experimental research and theoretical models have been devoted to study ion-solid interactions since the early days of ion physics. The ionizing radiation deposits energy in materials mainly through electronic excitation and ionization. Accurate characterization of the electronic stopping power is of essential importance to radiation damage research. With the advent of the numerical electronic structure methods, it is able to obtain electronic stopping power nonperturbatively and in a fully atomistic fashion [9]. In the low-velocity regime,

the study of the electronic stopping power is important for understanding the nonadiabatic coupling between ions and electrons [10], which was shown to be associated with the electronic band structure of the host materials [11,12]. In this regime, the electronic stopping power is dominated by the interaction between projectiles and valence electrons. Modeling valence electrons as a free electron gas (FEG) [13–16], the electronic stopping power is proportional to ion velocity; the experimental results of many metals provide strong evidence for this model [17–19].

There is an explicit band gap between the valence band maximum (VBM) and the conduction band minimum (CBM) of semiconductors and insulators, and a minimum energy is required by the valence electrons to pass through the band gap and be excited to the conduction band. Hence there is a threshold velocity for  $S_e$  below which electronic excitations are suppressed. The  $S_e$  of insulators and semiconductors has been studied by experimental measurements and theoretical simulations, such as slow protons in LiF [9], KCl [20], SiO<sub>2</sub> [21], and Ge [11]. The  $S_e$  of these materials was found to exhibit a pronounced velocity threshold, and then continues to increase in proportion to proton velocity.

For transition metals featuring a sharply peaked *d* band located below the Fermi energy, such as Cu [22], Au, Ag, and Zn [23–25], the  $S_e$  of these metals for slow light ions was found to exhibit deviations from velocity proportionality when the projectile velocity exceeds the excitation threshold of *d* electrons. In studying H ions in Zn and In, Goebel *et al.* [26] showed that the  $S_e$  of Zn and In for protons deviates from

\*Corresponding author: [maofei@mail.bnu.edu.cn](mailto:maofei@mail.bnu.edu.cn)

velocity proportionality towards higher values at ion velocities above 0.2 a.u., which is believed to be caused by excitation of  $d$  electrons of the media. However, for  $S_e$  of transition metal oxides, whether the deviation can still be retained is an open issue worth paying attention to, and research data on this aspect are relatively scarce. Roth *et al.* [27] measured the electronic stopping cross section of slow protons in ZnO, and found the electronic stopping shows a steeper slope at  $v \geq 0.25$  a.u., which is thought of as the result of zinc  $d$ -band electron excitation.

In the middle- and high-velocity regimes, the energy loss is predominant by electronic stopping. Because of the high-energy transfer rate in this velocity regime, the dependence of electronic excitations on the band gap of materials can be ignored, and the contribution of inner shell electrons to  $S_e$  has become an interesting issue in recent years. The processes of projectiles shooting through materials were studied by real-time time-dependent density functional theory (RT-TDDFT) combined with the projector augmented wave (PAW) formalism [28] or Gaussian augmented plane-wave method (GAPW) [29]; the contribution of core electrons of the target to electronic stopping was obtained. Ullah *et al.* [30] studied Ni projectiles in bulk Ni within the RT-TDDFT based pseudopotential scheme including core electron shells and showed that the excitation of core electrons plays a crucial role on the  $S_e$  in the middle- and high-velocity regions. Yao *et al.* [31] simulated the irradiation process of energetic protons in water and the results showed that the contribution of oxygen  $1s$  electrons to the electronic stopping reaches about 30% for impact velocity above 6.0 a.u. Recently, Lohmann *et al.* [32] performed experiments on irradiating single crystal silicon with protons and helium ions. By comparing the results obtained from channeling and off-channeling incident geometries, the relative contribution of the core electron excitation to the electronic stopping versus the projectile velocity is qualitatively given, and a meaningful insight is provided into core electron excitation under ion irradiation.

In this work, we investigated the  $S_e$  of channeling and off-channeling protons in ZnO by performing RT-TDDFT simulations, and systematically studied the roles played by zinc  $d$  electrons on  $S_e$  in a wide range of velocities. The threshold velocity and the deviation from the velocity-proportional  $S_e$  of ZnO are reproduced in the low-velocity regime. Moreover, we showed the energy distribution of holes and excited electrons after protons irradiating ZnO.

## II. METHOD AND COMPUTATIONAL DETAILS

The stopping processes of protons traversing ZnO are simulated by real-time time-dependent density-functional theory coupled with Ehrenfest molecular dynamics. The sphalerite structured zinc oxide is modeled by a  $2 \times 2 \times 2$  supercell (cubic lattice constant 4.63 Å) containing 64 atoms. The supercell size was chosen so as to minimize the spurious effects of the repetition while keeping manageable computational demands. Periodic boundary conditions are used throughout the simulations. A single  $k$  point ( $\Gamma$ ) is used for integrations in the Brillouin zone. We also tested for  $k$ -point convergence in a  $(2 \times 2 \times 2)$  Monkhorst-Pack grid, for some selected velocities with negligible differences of less than 2%. Norm-

conserving Troullier-Martins pseudopotentials [33] are used to describe the potential acting on the electrons given by the ionic system for the projectile and host atoms in this simulation. In order to explore the effect of semicore electrons of zinc on the electronic energy loss, we constructed two pseudopotential models for the zinc atom with two electrons ( $[\text{Ar}3d^{10}4s^2]$ ) as well as 12 electrons ( $[\text{Ar}]3d^{10}4s^2$ ) in the valence shell. The local-density approximation (LDA) with Perdew-Wang analytic representation [34] is employed for the exchange-correlation potential in our work. The external potential, electron density, and Kohn-Sham orbitals are discretized in a set of mesh grid points with uniform spacing of 0.16 Å along all three spatial coordinates in real space in the simulation cell. The initial ground-state Kohn-Sham orbitals are set up by diagonalization of the time-independent Kohn-Sham Hamiltonian for ZnO, and the initial wave function is constructed by linear combination of the atomic orbital method.

The ground-state Kohn-Sham orbitals serve as initial states for time-dependent simulations. Once the ground state of the system is known, the projectile located on the surface of the simulation box is given a constant velocity. The Kohn-Sham orbitals are propagated according to the time-dependent Kohn-Sham equation using the approximated enforced time-reversal symmetry (AETRS) method [35]; the time-dependent Kohn-Sham equations are

$$i \frac{\partial}{\partial t} \varphi_i(\mathbf{r}, t) = \left[ -\frac{\hbar^2}{2m} \nabla^2 + V_{\text{KS}}(\mathbf{r}, t) \right] \varphi_i(\mathbf{r}, t). \quad (1)$$

The Kohn-Sham potential  $V_{\text{KS}}(\mathbf{r}, t)$  is conventionally separated in the following way:

$$V_{\text{KS}}(\mathbf{r}, t) = V_{\text{ext}}(\mathbf{r}, t) + V_{\text{H}}(\mathbf{r}, t) + V_{\text{XC}}(\mathbf{r}, t), \quad (2)$$

where  $V_{\text{ext}}(\mathbf{r}, t)$  is the time-dependent electron-nucleus potential,  $V_{\text{H}}(\mathbf{r}, t)$  is the Hartree potential, and  $V_{\text{XC}}(\mathbf{r}, t)$  presents the time-dependent exchange-correlation potential. The electron density of the system can be obtained from the time-dependent Kohn-Sham orbitals

$$\rho(\mathbf{r}, t) = 2 \sum_i^{\text{occ}} |\varphi_i(\mathbf{r}, t)|^2. \quad (3)$$

The propagation step length  $\Delta t \times v \sim 1.44 \times 10^{-3}$  Å is adopted for various velocities to ensure the energy convergence of time-dependent evolution. All simulations are carried out by the OCTOPUS code [36,37].

In the channeling geometry, the projectile is moving along [001] crystal axis (called hyperchanneling) with constant velocity by neglecting forces on the projectile. In our simulations, all host atoms are fixed at their equilibrium positions, so the projectile energy is transferred only through inelastic scattering to the electronic subsystem of ZnO. In any case, the projectile velocities are fast enough to leave little or no time for the nuclei to respond. The total energy of the system (or the electronic energy of ZnO) changes as a function of the projectile position in the simulations. This allows us to extract the  $S_e$  by a linear fit of the total energy of the system with respect to the projectile position. In order to investigate the influences of the impact parameter on the stopping power, we

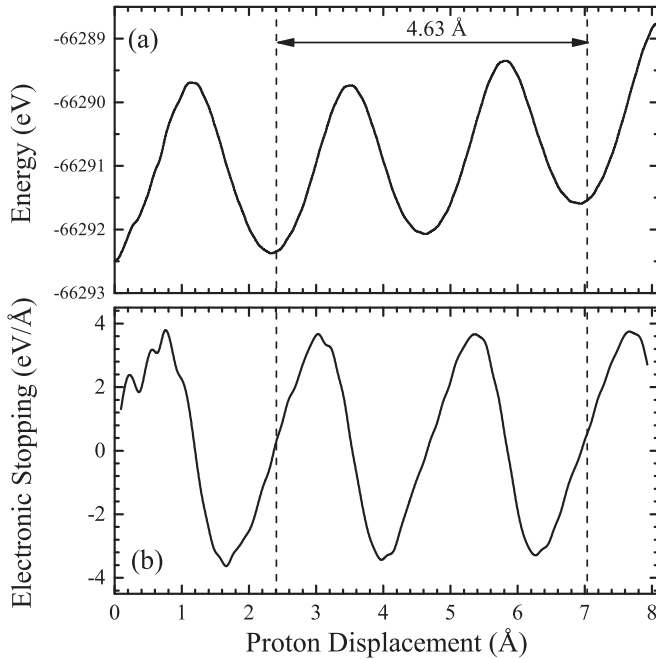


FIG. 1. (a) Total energy and (b) instantaneous electronic stopping power as a function of proton displacement along the center channeling trajectory at velocity of 0.1 a.u.

studied two trajectories depending on the impact parameter shown in the insets of Fig. 2.

In the off-channeling case, the projectiles take random incident directions, and a bigger  $2 \times 2 \times 4$  supercell containing 128 atoms is employed for simulations. For off-channeling trajectories we chose three directions [0.304, 0.047, 0.952], [0.317, 0.320, 0.893], and [0.444, 0.513, 0.735] (given normalized here), which were established randomly based on uniform sampling and an immediate head-on collision was avoided. Four initial incident positions are selected for each direction. So, there are 12 off-channeling trajectories for each velocity; we get the electronic stopping power of each trajectory by averaging the instantaneous stopping power and the stopping power of off-channeling geometry is obtained by averaging the 12 trajectories' results for each velocity. It should be noted that the charge state of the projectile moving through ZnO is not an input, which is part of the solution to the TDDFT calculation.

### III. RESULTS AND DISCUSSION

Figure 1(a) shows the evolution of total energy of the system as the proton displacement. At impact velocity 0.1 a.u., a small amount of energy is transferred to the electronic system of ZnO, approaching the case of adiabatic behavior. As shown in Fig. 1(a), the total energy of the system oscillates with the projectile displacement. The oscillation of the total energy reflects the periodicity of the lattice structure of ZnO. Therefore, it becomes more challenging for accurately extracting the average electronic stopping in this energy range. The instantaneous  $S_e$  is defined by the slope of the total energy vs projectile displacement, as shown in Fig. 1(b). The instantaneous electronic stopping shows “unsteady fluctua-

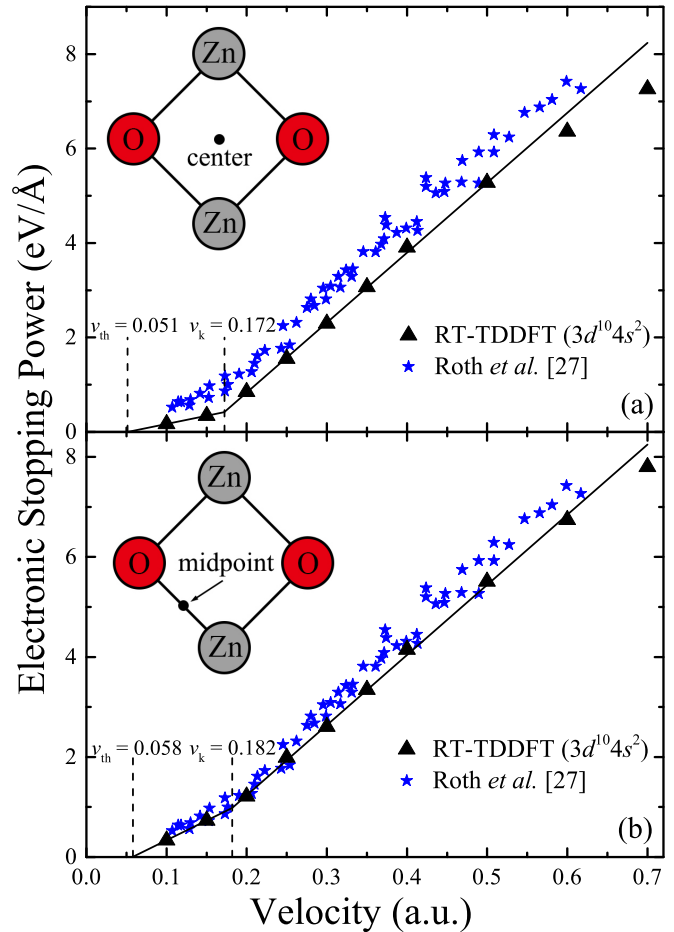


FIG. 2. Electronic stopping power as a function of velocity of protons moving along (a) the center and (b) the midpoint channeling trajectories, respectively. The solid lines are the linear fitting of triangles. The experimental data are from Ref. [27]. The insets show the top view of the incidence geometries of channeling trajectories. The gray circles indicate zinc atoms, the red circles present oxygen atoms, and the black circles show the incident positions.

tions” at the beginning of the collisions, which we interpret as an influence of the charge transfer of the bare proton and a transient produced by the sudden entrance of the projectile [22,38]. In order to avoid the effects of the transient state and charge capture on the electronic stopping, we extracted the  $S_e$  after the instantaneous  $S_e$  stabilizes. During the steady stage,  $S_e$  is obtained by averaging the instantaneous electronic stopping over two entire periods as indicated by the vertical dashed lines in Fig. 1, which helps to accurately determine the equilibrium electronic stopping power, and the influence of the adiabatic behavior on the equilibrium electronic stopping power is completely offset.

The  $S_e$  of ZnO for protons moving along the center channeling trajectory obtained from RT-TDDFT calculations is shown in Fig. 2(a), as well as the experimental data reported in Ref. [27]. The incident position is displayed in the inset of Fig. 2(a). Overall, the calculated results from hyperchanneling trajectories are lower than the experimental measurements. This is because the protons are farthest from the host atoms and the electron density experienced by the projectiles is

the lowest in this channeling trajectory. For the  $S_e$  obtained from RT-TDDFT simulations, three regimes are found. In the first regime, the  $S_e$  is zero at  $v \leq 0.051$  a.u. by linearly extrapolating the TDDFT simulation results to lower energies. This is ascribed to the band gap of ZnO which results in a threshold velocity in the electronic stopping. So, the threshold velocity  $v_{th}$  for the  $S_e$  of protons channeling along the center trajectory is at 0.051 a.u., which is in a quantitative agreement with the experimental value 0.055 a.u. [27]. In the second velocity regime  $0.051 < v < 0.172$  a.u., the  $S_e$  is proportional to the proton velocity. In this regime, the electrons lying at the VBM of ZnO get excited as the proton velocity exceeds the threshold velocity, and there are mainly six valence electrons including zinc  $4s$  electrons and oxygen  $2p$  electrons per ZnO unit participating in the excitation. The generation of electron-hole pairs is the main energy loss channel. There is a sharp peak formed by the semicore  $3d$  electrons of zinc in the density of states below the VBM of ZnO [39], and the peak-lying electrons get to be excited in the third velocity regime  $0.172 < v < 0.6$  a.u. There are 16 electrons per ZnO unit including also zinc  $3d$  electrons joining in the stopping processes in this velocity regime; an additional energy is required to produce more electron-hole pairs, giving rise to an increase in the electronic energy loss. Therefore, the  $S_e$  is proportional to the proton velocity with a steeper slope. The velocity for the transition between the two velocity scaling regimes is referred to as kink velocity  $v_k$ . So, our calculated  $v_k$  is 0.172 a.u. in this channeling case, which is smaller than the experiment data 0.25 a.u. reported in Ref. [27].

Figure 2(b) shows the  $S_e$  of protons traversing along the midpoint channeling trajectory of ZnO [see the inset of Fig. 2(b)]. Compared to the center trajectories, the projectile approaches the nuclei of host atoms closer under this incidence condition and the simulation results are becoming consistent with the measured data. It can be seen from Fig. 2(b) that three regimes of the  $S_e$  are still present in the center trajectory. The  $v_{th}$  is at 0.058 a.u., which is in a good agreement with experiments [27], and the  $v_k$  is 0.182 a.u., which is closer to the experimental value than that obtained in the center trajectory.

The  $v_{th}$  is 0.051 and 0.058 a.u. for center and midpoint trajectories, respectively. This demonstrates that  $v_{th}$  is insensitive to the impact parameter, which suggests that the zinc  $4s$  electrons are uniformly distributed in the channel of ZnO. The  $v_k = 0.172$  and 0.182 a.u. for center and midpoint trajectories, respectively, which is more sensitive to the impact parameter. This is consistent with the fact that the inner electron excitation is strongly dependent on the impact parameter.

For the off-channeling trajectory, the low-energy electronic stopping power with  $3d$  electrons being explicitly considered is shown in Fig. 3. The agreement between our simulation results and the measured data is noticeable. It is necessary to consider the off-channeling geometries to obtain the electronic stopping power in comparison with the experimental value. Since the off-channeling stopping is the statistical averaging of multiple trajectories, due to the error bars, it is hard to determine the threshold velocity and the kink velocity as accurately as in the channeling trajectories.

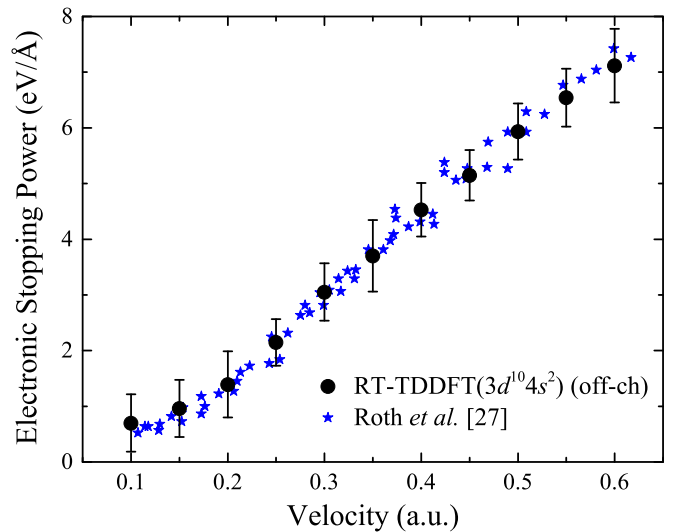


FIG. 3. Electronic stopping power as a function of velocity of protons traveling along the off-channeling trajectory in ZnO.

The  $S_e$  is extended to the velocity of 4.0 a.u. and the results are shown in Fig. 4. For the channeling case, it can be seen from the figure that the contribution of semicore  $3d$  electrons to the electronic stopping is negligible in the low-velocity regime ( $v < 0.5$  a.u.). However, the  $S_e$  deviates from the experimental data and the SRIM predictions [40] towards lower values as the velocity continues to increase. In the case of the center trajectory, the channeling stopping including only  $4s$  electrons is lower than the experimental data [41] by 69.9% at 4.0 a.u., while the excitation of  $d$  electrons increases the  $S_e$  by 45.4% ( $S_e$  is increased by 1.63 eV/Å). In the case of the midpoint trajectory, the  $S_e$  including only  $4s$  electrons is lower by 64.2% in comparison with the experimental result at 4.0 a.u.,

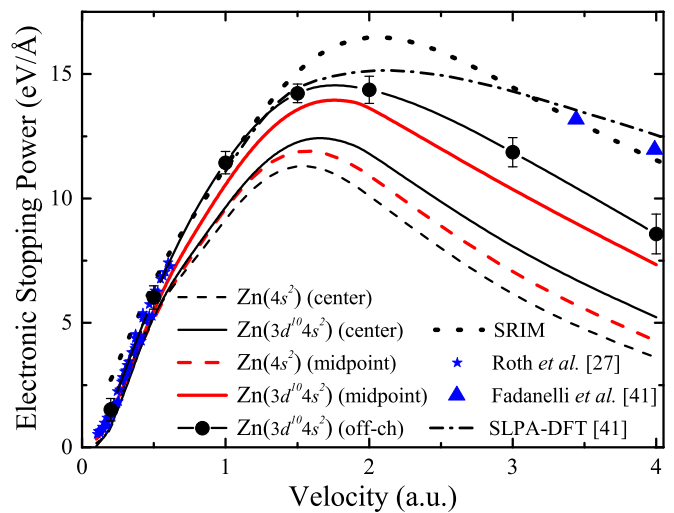


FIG. 4. Electronic stopping powers obtained from RT-TDDFT calculations are shown as a function of proton velocity for channeling (including both center and midpoint trajectories, and considering  $3d^{10}$  electrons or not) and off-channeling trajectories, together with SRIM predictions, experimental data from Refs. [27,41], and SLPA-DFT calculations from Ref. [41].

but the  $S_e$  is enhanced by 71.5% (increased by 3.06 eV/Å) with  $d$ -electron excitation being taken into consideration.

The results obtained from channeling trajectories point to some important arguments regarding the underlying mechanisms of electronic stopping. (i) Under the center incidence condition, the excitation of semicore  $3d$  electrons significantly contributes to the  $S_e$  in the velocity range from 0.5 to 4.0 a.u. This means that the semicore  $3d$  electrons are indispensable to describe the  $S_e$  even under the maximum impact parameter. It is different from the case of aluminum, in which the inner electrons have a negligible influence on  $S_e$  of the hyperchanneling trajectory with the maximum impact parameter [42]. (ii) Under the center trajectory condition, zinc  $3d$  electrons contribute about 1.5 eV/Å beyond the Bragg peak, while this contribution is increased by about 3.0 eV/Å in the midpoint trajectory, indicating that the excitation of  $3d$  electrons strongly depends on the impact parameter and makes a significant contribution to the electronic stopping. (iii) We noticed that the Bragg peaks of  $S_e$  are located at 1.5 a.u. for both center and midpoint trajectories with zinc containing only  $4s$  electrons in the valence shell, which are located at 1.7 a.u. for both trajectories including also  $3d$  electrons. So, the stopping maximum position is related to the number of electrons involved in the electron stopping dynamics.

The SRIM model is based on extending the Lindhard-Schiott theory with inputs from available experimental data and it is widely used as a standard reference. In general, the electronic stopping power obtained from channeling trajectories is lower than the experimental data and the SRIM predictions, especially in the high-velocity range [12,22,29]. The  $S_e$  obtained from off-channeling geometry (see the circles in Fig. 4) is greatly improved compared to the channeling geometry, approaching the SRIM results. The off-channeling stopping power is increased by 12.5% in comparison with that obtained from the midpoint trajectory including  $d$  electrons at 0.5 a.u. So, it is necessary to consider the off-channeling geometry to meet the measured data. The agreement of the off-channeling results with the SRIM and the measured data is more excellent than the channeling ones up to 1.5 a.u. Under real irradiation conditions, the projectiles move uncontrollably in materials, inevitably exploring the core regions of host atoms, which is similar to the off-channeling situation [43]. As the projectile approaches the nuclei of the host atoms, it experiences higher electron density since core electrons are highly localized distributed around the nuclei, resulting in more efficient electronic excitations in the off-channeling trajectories. However, this agreement fails beyond the Bragg peak. The semiempirical code SRIM employs Bragg rule to describe the stopping power of ZnO; Fadanelli *et al.* [41] confirmed that the electronic stopping maximum given by the Bragg rule is larger than calculations by using molecular electronic states. This may be one of the reasons why our simulation results are lower than SRIM data near the stopping maximum.

Figure 4 also displays the stopping power of ZnO for protons obtained from the shellwise local plasma approximation together with the density functional theory (SLPA-DFT) calculations [41], in which the contributions from all electron shells of ZnO are considered. Our off-channeling stopping powers are in good agreement with SLPA-DFT calculations

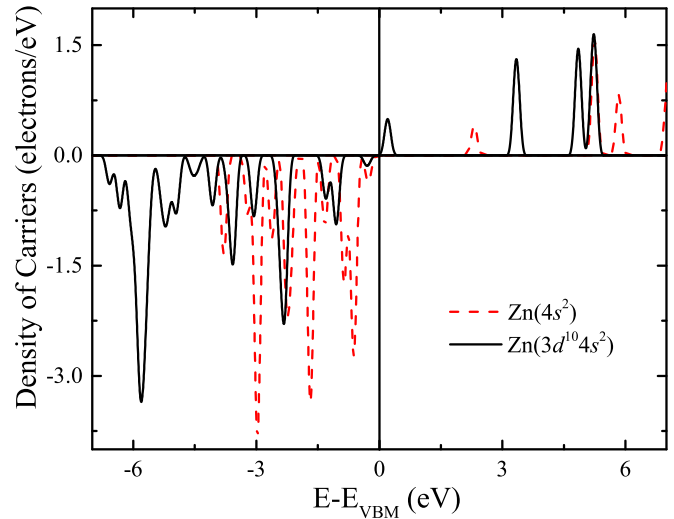


FIG. 5. Density of carrier population as a function of energy for 0.5 a.u. proton channeling along the midpoint trajectory for both pseudopotentials. The positive and negative values show the density of excited electrons and holes, respectively.  $E_{\text{VBM}}$  represents the energy of VMB of ZnO.

up to the stopping maximum, but the off-channeling results begin to deviate from the SLPA-DFT results as the velocity continues to increase, indicating that more core electrons of the host atoms are required to be explicitly considered in order to obtain calculation results that are in line with experimental data. It was demonstrated that oxygen  $1s$  electrons make a significant contribution to the  $S_e$  of water [31]. In oxides, such as ZnO, the question of whether oxygen  $1s$  electrons should be considered in the electronic stopping is worth further investigation. In addition, the size of the supercell also affects the  $S_e$  results, as excitation of plasmons with wavelengths longer than the simulation cell cannot be described correctly [42]. This is out of the scope of this paper.

In order to provide insight into the underlying physics of  $d$  electron excitation, the occupation of electronic states in the valence band and conduction band is obtained by projecting the time-dependent Kohn-Sham (TDKS) wave functions  $\psi_j(t)$  at the final step of the TDDFT simulation onto the ground-state Kohn-Sham orbitals  $\varphi_i$  of ZnO [44] as

$$n_{\text{occ}}(\varepsilon_i) = \sum_j f_j |\langle \varphi_i | \psi_j(t) \rangle|^2, \quad (4)$$

and the population of holes and excited electrons is obtained as follows:

$$P_{h,e}(\varepsilon_i) = n_{\text{occ}}(\varepsilon_i) - f_i |\langle \varphi_i | \varphi_i \rangle|^2, \quad (5)$$

where  $\varepsilon_i$  represents the eigenenergy of the  $i$ th Kohn-Sham state and  $f_i$  is the fixed occupation of the Kohn-Sham state  $\psi_i$  ( $f = 2$  for occupied states or 0 for otherwise). The negative and the positive values of  $P_{h,e}[\varepsilon(i)]$  represent the occupation of holes and excited electrons, respectively. The density distribution of holes and excited electrons is shown in Fig. 5. It can be seen from the figure that the holes are mainly produced in the range of 4 eV below the VBM when  $3d$  electrons are frozen, while the hole energy expands up to 7 eV below the VBM when  $3d$  electrons participate in the

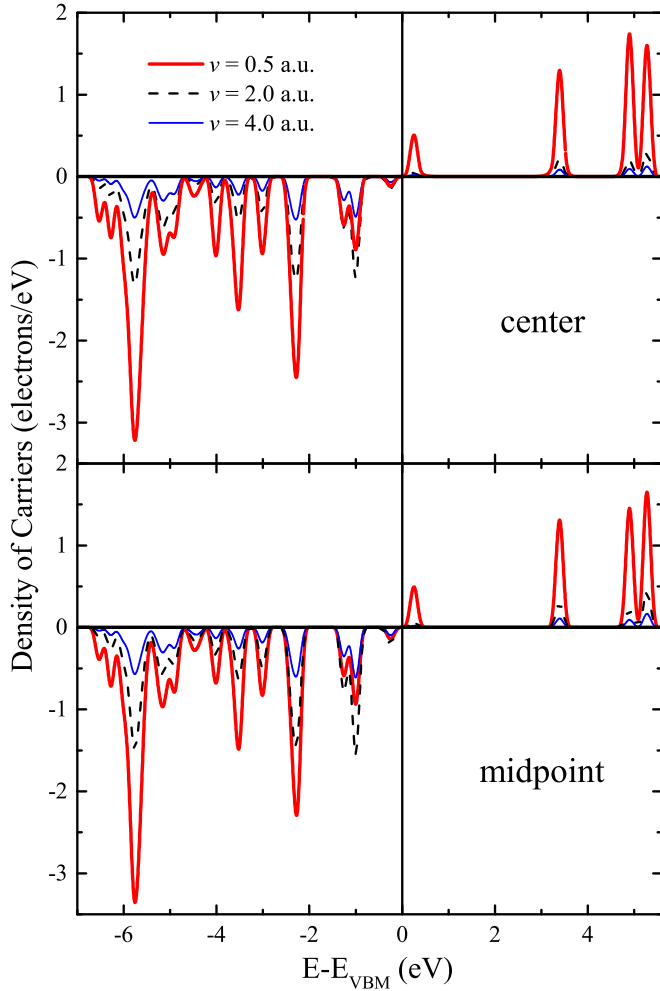


FIG. 6. Density of carrier population as a function of energy for protons channeling along center (upper panel) and midpoint (lower panel) trajectories with zinc containing also 3d electrons. The negative and positive values refer to the density of holes and excited electrons, respectively.  $E_{\text{VBM}}$  represents the energy of VMB of ZnO.

electronic stopping. Therefore, the distribution of holes is broadened by the presence of 3d electrons. Since the energy distribution of excited electrons is broad and some of them are ionized, the number of electrons that leave the holes cannot be explicitly counted by the discrete unoccupied states. We integrated the hole density over the whole energy range, and the total number of holes produced in the supercell is 3.45 and 3.5 for including *d* electrons or not, respectively. This indicates that the presence of 3d electrons does not appreciably provide additional holes, but changes the excitation spectrum of valence electrons, thereby moving forward the position of the stopping maximum.

Figure 6 shows the energy distribution of holes and excited electrons under different velocities and trajectories. As the velocity increases ( $v > 0.5$  a.u.), the response time of electrons is limited and the number of holes and excited electrons decreases. However, the electronic stopping at 0.5 a.u. is lower than that at 2.0 a.u., which is not in line with what often assumed the hole generation is to be directly proportional to the electronic stopping power. In the high-velocity regime (beyond the Bragg peak), the number of holes produced is almost the same for the center and midpoint trajectories at a given velocity, but the  $S_e$  obtained from both trajectories is significantly different. This is because the  $S_e$  is not only related to the number of electrons excited, but also related to the energy spectra of holes and excited electrons [45]. We calculated the average energy of excited (ionized) electrons; the results show that the energy of excited (ionized) electrons produced in the midpoint trajectory is higher than that produced in the center trajectory at higher velocities. It may be explained by the fact that the probability of ion-electron scattering becomes higher at smaller impact parameters and more electrons are excited to the high-lying states or ionized by stronger ion-electron scattering.

#### IV. CONCLUSIONS

In summary, we studied the electronic stopping power of energetic protons moving through zinc oxide along the channeling and off-channeling trajectories within the framework of RT-TDDFT. In the low-velocity range, the calculated threshold velocity agrees well with the experimental measurement. The experimentally observed deviation from the velocity-proportional electronic stopping power of ZnO for protons is reproduced. We also calculated the energy distribution of excited electrons and holes after collisions, and tested out that the electronic energy loss of protons is related to the number as well as the energy spectra of holes and excited electrons.

Our RT-TDDFT stopping power results for channeling trajectories are lower than the experimental data beyond 0.5 a.u., while the stopping powers obtained from the off-channeling geometry are significantly improved and they are in good agreement with the experimental values up to the stopping maximum. Our simulation results showed that the excitation of semicore 3d electrons is strongly dependent on the impact parameter and zinc 3d-electron excitation contributes substantially to the electronic stopping power in the high-energy range.

#### ACKNOWLEDGMENTS

Dr. C.-Z. Gao is thanked for stimulating discussion on this work. This work is supported by the National Natural Science Foundation of China under Grants No. 11975119, No. 11505092, and No. 11774030. B.-S.L. acknowledges Sichuan Science and Technology Program (Grant No. 2020ZYD055) for financial support.

[1] C. W. Lee, J. A. Stewart, R. Dingreville, S. M. Foiles, and A. Schleife, *Phys. Rev. B* **102**, 024107 (2020).

[2] M. V. Moro, P. Bauer, and D. Primetzhofer, *Phys. Rev. A* **102**, 022808 (2020).

- [3] E. E. Quashie, R. Ullah, X. Andrade, and A. A. Correa, *Acta Mater.* **196**, 576 (2020).
- [4] J. Halliday and E. Artacho, *Phys. Rev. B* **100**, 104112 (2019).
- [5] P. D. Townsend, *Rep. Prog. Phys.* **50**, 501 (1987).
- [6] S. Duzellier, *Aerosp. Sci. Technol.* **9**, 93 (2005).
- [7] A. C. Begg, F. A. Stewart, and C. Vens, *Nat. Rev. Cancer* **11**, 239 (2011).
- [8] A. Verkhovtsev, E. Surdutovich, and A. V. Solov'yov, *Sci. Rep.* **6**, 27654 (2016).
- [9] J. M. Pruneda, D. Sanchez-Portal, A. Arnau, J. I. Juaristi, and E. Artacho, *Phys. Rev. Lett.* **99**, 235501 (2007).
- [10] A. Tamm, M. Caro, A. Caro, and A. A. Correa, *Phys. Rev. B* **99**, 174302 (2019).
- [11] R. Ullah, F. Corsetti, D. Sánchez-Portal, and E. Artacho, *Phys. Rev. B* **91**, 125203 (2015).
- [12] E. E. Quashie and A. A. Correa, *Phys. Rev. B* **98**, 235122 (2018).
- [13] E. Fermi and E. Teller, *Phys. Rev.* **72**, 399 (1947).
- [14] R. H. Ritchie, *Phys. Rev.* **114**, 644 (1959).
- [15] P. M. Echenique, R. M. Nieminen, and R. H. Ritchie, *Solid State Commun.* **37**, 779 (1981).
- [16] P. M. Echenique, F. Flores, and R. H. Ritchie, *Solid State Phys.* **43**, 229 (1990).
- [17] G. Martínez-Tamayo, J. C. Eckardt, G. H. Lantschner, and N. R. Arista, *Phys. Rev. A* **54**, 3131 (1996).
- [18] D. Primetzhofer, S. Rund, D. Roth, D. Goebel, and P. Bauer, *Phys. Rev. Lett.* **107**, 163201 (2011).
- [19] A. A. Correa, J. Kohanoff, E. Artacho, D. Sánchez-Portal, and A. Caro, *Phys. Rev. Lett.* **108**, 213201 (2012).
- [20] S. N. Markin, D. Primetzhofer, and P. Bauer, *Phys. Rev. Lett.* **103**, 113201 (2009).
- [21] F. Mao, C. Zhang, J. Dai, and F. S. Zhang, *Phys. Rev. A* **89**, 022707 (2014).
- [22] E. E. Quashie, B. C. Saha, and A. A. Correa, *Phys. Rev. B* **94**, 155403 (2016).
- [23] E. D. Cantero, G. H. Lantschner, J. C. Eckardt, and N. R. Arista, *Phys. Rev. A* **80**, 032904 (2009).
- [24] S. N. Markin, D. Primetzhofer, M. Spitz, and P. Bauer, *Phys. Rev. B* **80**, 205105 (2009).
- [25] D. Goebel, D. Roth, and P. Bauer, *Phys. Rev. A* **87**, 062903 (2013).
- [26] D. Goebel, W. Roessler, D. Roth, and P. Bauer, *Phys. Rev. A* **90**, 042706 (2014).
- [27] D. Roth, B. Bruckner, G. Undeutsch, V. Paneta, A. I. Mardare, C. L. McGahan, M. Dosmailov, J. I. Juaristi, M. Alducin, J. D. Pedarnig, R. F. Haglund, Jr., D. Primetzhofer, and P. Bauer, *Phys. Rev. Lett.* **119**, 163401 (2017).
- [28] A. Ojanperä, A. V. Krasheninnikov, and M. Puska, *Phys. Rev. B* **89**, 035120 (2014).
- [29] D. C. Yost and Y. Kanai, *Phys. Rev. B* **94**, 115107 (2016).
- [30] R. Ullah, E. Artacho, and A. A. Correa, *Phys. Rev. Lett.* **121**, 116401 (2018).
- [31] Y. Yao, D. C. Yost, and Y. Kanai, *Phys. Rev. Lett.* **123**, 066401 (2019).
- [32] S. Lohmann and D. Primetzhofer, *Phys. Rev. Lett.* **124**, 096601 (2020).
- [33] N. Troullier and J. L. Martins, *Phys. Rev. B* **43**, 1993 (1991).
- [34] J. P. Perdew and Y. Wang, *Phys. Rev. B* **45**, 13244 (1992).
- [35] A. Castro, M. A. L. Marques, and A. Rubio, *J. Chem. Phys.* **121**, 3425 (2004).
- [36] X. Andrade, J. Alberdi-Rodriguez, D. A. Strubbe, M. J. T. Oliveira, F. Nogueira, A. Castro, J. Muguerza, A. Arruabarrena, S. G. Louie, A. Aspuru-Guzik, A. Rubio, and M. A. L. Marques, *J. Phys.: Condens. Matter* **24**, 233202 (2012).
- [37] X. Andrade, D. A. Strubbe, U. De Giovannini, A. H. Larsen, M. J. T. Oliveira, J. Alberdi-Rodriguez, A. Varas, I. Theophilou, N. Helbig, M. Verstraete, L. Stella, F. Nogueira, A. Aspuru-Guzik, A. Castro, M. A. L. Marques, and A. Rubio, *Phys. Chem. Chem. Phys.* **17**, 31371 (2015).
- [38] A. Kononov and A. Schleife, *Phys. Rev. B* **102**, 165401 (2020).
- [39] H. Dixit, R. Saniz, D. Lamoen, and B. Partoens, *J. Phys.: Condens. Matter* **22**, 125505 (2010).
- [40] J. F. Ziegler, M. Ziegler, and J. Biersack, *Nucl. Instrum. Methods Phys. Res., B* **268**, 1818 (2010).
- [41] R. C. Fadanelli, C. D. Nascimento, C. C. Montanari, J. C. Aguiar, D. Mitnik, A. Turos, E. Guziewicz, and M. Behar, *Eur. Phys. J. D* **70**, 178 (2016).
- [42] A. Schleife, Y. Kanai, and A. A. Correa, *Phys. Rev. B* **91**, 014306 (2015).
- [43] J. J. Dorado and F. Flores, *Phys. Rev. A* **47**, 3062 (1993).
- [44] T. Otobe, M. Yamagiwa, J. I. Iwata, K. Yabana, T. Nakatsukasa, and G. F. Bertsch, *Phys. Rev. B* **77**, 165104 (2008).
- [45] D. C. Yost and Y. Kanai, *J. Am. Chem. Soc.* **141**, 5241 (2019).